Dynamic imaging in electrical capacitance tomography and electromagnetic induction tomography using a Kalman filter

Meas. Sci. Technol. **18** (2007) 3287–3294 doi:10.1088/0957-0233/18/11/004

Dynamic imaging in electrical capacitance tomography and electromagnetic induction tomography using a Kalman filter

Manuchehr Soleimani[1], Marko Vauhkonen[2], Wuqiang Yang[3], Anthony Peyton[3], Bong Seok Kim[4] and Xiandong Ma[3]

[1] William Lee Innovation Centre, School of Materials, The University of Manchester, PO Box 88, Manchester M60 1QD, UK
[2] Philips Research Europe, Medical Signal Processing, Weisshausstrasse 2, D-52066 Aachen, Germany
[3] School of Electrical and Electronic Engineering, The University of Manchester, PO Box 88, Manchester M60 1QD, UK
[4] Biomedical Engineering Branch, National Cancer Center, Goyang-si, Gyeonggi-do 410-769, Korea

E-mail: M.Soleimani-2@manchester.ac.uk

Received 5 February 2007, in final form 30 May 2007
Published 20 September 2007
Online at stacks.iop.org/MST/18/3287

Abstract
Electrical capacitance tomography (ECT) and electromagnetic induction tomography (EMT) attempt to visualize the distributions of materials with different permittivity and conductivity/permeability, aiming to reveal electrical and magnetic characteristics of an object, by measuring electrical capacitance and electromagnetic inductance on the periphery of the object. In ECT, capacitances of pairs of electrodes placed around the periphery are measured and in EMT, mutual induction of pairs of coils is measured. In this paper, a dynamic imaging technique is developed for ECT and EMT with a linearized Kalman filter to improve the temporal resolution of images. The inverse problem is treated as a state estimate. A Kalman estimator is used to obtain the material distribution. Experimental results demonstrate that the dynamic imaging technique can improve the spatio-temporal resolution of both ECT and EMT.

Keywords: electrical capacitance tomography, electromagnetic induction tomography, permittivity and conductivity distribution, inverse problem, dynamic imaging, Kalman filter

(Some figures in this article are in colour only in the electronic version)

1. Introduction

Electrical capacitance tomography (ECT) and electromagnetic induction tomography (EMT) have great potential for industrial and biomedical applications as both techniques are non-invasive, and can be used to monitor fast-moving processes. ECT is a relatively mature modality of industrial process tomography (Yang and Peng 2003). The aim of ECT is to visualize the distribution of dielectric materials with a contrast in permittivity, by applying electric fields and measuring the capacitances from a set of electrodes. Applications of ECT include the measurement of gas–oil flows in pipelines and gas–solid flows in pneumatic conveyors. EMT attempts to reveal the distribution of electromagnetic characteristics of the materials, especially the permeability and/or conductivity distributions, by applying magnetic

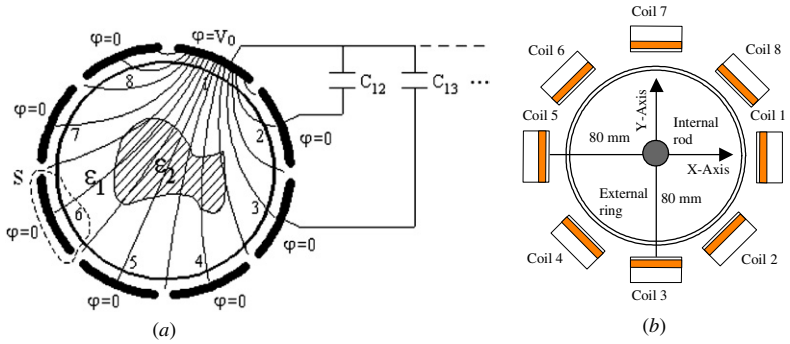

Figure 1. Typical ECT and EMT sensors. (*a*) Eight-electrode ECT sensor, with electric field lines shown and (*b*) eight-coil sensor array, with object space enclosed by an insulating tube.

excitation (Griffiths 2001, Merwa *et al* 2005). A set of excitation coils is used to generate a magnetic field, and the secondary eddy current produced within the conductive object is detected by sensing coils.

Image reconstruction with both ECT and EMT is an ill-posed inverse problem. Traditionally, the tomographic imaging techniques are classified into three categories: (1) static imaging, (2) difference imaging and (3) dynamic imaging. In the static case, an image is produced using a single set (i.e. frame) of data, which gives the actual permittivity, permeability or conductivity distribution of the object. By the difference imaging, the change in permittivity or conductivity is reconstructed between two time steps. The dynamic imaging technique attempts to reveal the dynamic behaviour of the object as an image is reconstructed using one pattern of measurement data.

While advances have been made in static image reconstruction for ECT and EMT using both simulation and experimental data, little work has been done on dynamic imaging for either technique. For example, the static imaging technique fails to produce satisfactory images of a liquid metal flow due to the fast changes in conductivity (Soleimani *et al* 2006). As a result, the information on the temporal evolution of the conductivity distribution is lost or corrupted.

The Kalman filter can provide an optimal estimate of a dynamic state vector at each time step based on the knowledge of a random process, which causes the state to change. By formulating image reconstruction using a Kalman filter, the time resolution of the reconstructed images can be increased. A typical experiment in ECT or EMT alternately fires each excitation electrode (coils) and measures all of the sensing responses. In the static case, a complete set of data are used to reconstruct each frame. However, these measurements are actually described over time. Since the Kalman filter has an update model, each excitation can be treated as a separate frame. Although the measurements associated with this may be pertinent only to part of the data space, the Kalman filter optimally combines these with the stochastic state evaluation model.

Kalman filtering and dynamic imaging have been extensively studied in electrical impedance tomography (EIT) (Vauhkonen *et al* 1998a, 1998b, 2000, Kim *et al* 2004, 2006). A time-varying EIT problem has been solved by taking into account a fluid dynamic model (Seppänen *et al* 2007) for process tomography application.

This paper presents a dynamic imaging technique with a linearized Kalman filter (LKF) for online monitoring. The inverse problem is treated as a state estimate, and the time-varying state is estimated. Both ECT and EMT are considered and taken as separate examples. Despite their similarities, the two modalities are based on different governing equations. This demonstrates the broad applicability of the LKF approach. In addition, the use of the LKF as a combined tool for both the modalities is a step towards non-contact multi-modal tomography for fast-moving multiphase applications. This is the first study of dynamic imaging with EMT and the first LKF study of ECT using experimental data, as well as one of the first studies of dynamic imaging with ECT (Ijaz *et al* 2006, Watzenig *et al* 2004, 2007). In this paper, *a priori* information about the likely spatial structure of the reconstructed image is also incorporated. A smooth regularization for the spatial structure has been used. The experimental results with dynamic data sets are presented both for ECT and EMT.

2. ECT and EMT sensors and forward problems

2.1. ECT and EMT sensors

As is shown in figure 1(*a*), a typical ECT sensor comprises an array of conducting plate electrodes, which are mounted on the outside of a non-conducting pipe, and surrounded by an electrical shield (Yang 1996). For a metal wall pipe or vessel, the sensing electrodes must be mounted internally, with an insulation layer between the electrodes and the metal wall and using the metal wall as the electrical shield. Other components in the sensor include radial and axial screen electrodes, which are arranged to reduce the external coupling capacitance between the electrodes and to achieve an improved signal-to-noise ratio (SNR). In most applications, the electrodes do not have direct physical contact with the object material and consequently ECT is a non-intrusive and non-invasive modality, which avoids contamination of the materials.

An EMT sensor, as is shown in figure 1(*b*), is used to generate data for image reconstruction (Ma *et al* 2006). It consists of eight coils for excitation and detection. The inner diameter of the coils is 4 cm, the outer diameter is 5 cm and the length is 2 cm. The coils are arranged in a circular ring surrounding the object to be imaged. The distance between the centres of two opposite coils is 16 cm.

2.2. Forward problem in ECT

The forward problem in ECT is to estimate the capacitance for a given ECT sensor geometry, applied potential and permittivity distribution in the cross section of a sensor. While the conventional arrangement is to use a single electrode for excitation and a single electrode for detection, different measurement protocols have been attempted, e.g. a combination of electrodes. With the conventional protocol, each of the electrodes is set to some known potential in turn, while the other electrodes serve as detectors and remain a zero potential. The charge is measured on each of the detection electrodes. In figure 1(*a*), the electric field lines are shown. In each scan, a voltage $\varphi = v_l$ is applied to one electrode and the others are set to zero.

In general, the forward problem requires the solution of Maxwell's equations. At low frequencies, wave propagation and diffusion effects may be ignored. In a simplified mathematical model, the electrostatic approximation $\nabla \times E = 0$ is taken, which effectively ignores the effect of wave propagation. Let us take $E = -\nabla u$ and assume no internal charges. Then the following equation holds:

$$\nabla \cdot \varepsilon \nabla u = 0 \quad \text{in} \quad \Omega, \tag{1}$$

where ε is the relative permittivity, u is the electric potential and Ω is the region containing the field.

The potential on each electrode is known as

$$u = v_l \text{ on electrode } E_l, \tag{2}$$

where E_l is the lth electrode held at the potential v_l.

To solve equation (1) together with equation (2) numerically, the domain is partitioned into k tetrahedral with a total of n vertices. The permittivity coefficients are approximated by a piecewise constant function on that mesh. Given a standard nodal basis $\{\phi_i\}_{i=1}^n$ for the set of piecewise linear functions, a potential is sought in the form

$$u_h = \sum_{i=1}^{n} u_i \phi_i. \tag{3}$$

Multiplying the Poisson equation by an arbitrary, but sufficiently smooth test function v and integrating over Ω gives

$$\int_\Omega v \nabla \cdot (\varepsilon \nabla u_h)\, \mathrm{d}x^2 = 0. \tag{4}$$

By partial integration, the following equation is obtained:

$$\int_\Omega \varepsilon \nabla u_h \cdot \nabla v\, \mathrm{d}x^2 = \int_{\Gamma_1} \varepsilon \nabla u_h \cdot \tilde{n} v\, \mathrm{d}x + \int_{\Gamma 2} \varepsilon \nabla v \cdot \tilde{n} u_h\, \mathrm{d}x, \tag{5}$$

where Γ_1 is a part of the boundary, in which the flux is specified, and Γ_2 is a part of the boundary, where the voltage is given. Assuming $K(i, j) = \int_\Omega \varepsilon \nabla \phi_i \cdot \nabla \phi_j\, \mathrm{d}x^2$, $i, j = 1 : n$, a linear system of equations is obtained as

$$K(\varepsilon) U = B, \tag{6}$$

where the matrix K is the discrete representation of the operator $\nabla \cdot \varepsilon \nabla$ and the vector B is the voltage boundary condition term (i.e. the second term of the right side of equation (5)) and U is the vector of an electric potential solution.

In an actual ECT set-up (Yang and Peng 2003, Soleimani and Lionheart 2005), the mesh is extended beyond the electrodes. The voltage zero boundary condition is considered for the external screen, to reflect the grounded screens. Voltage v_l is considered for excitation electrodes and voltage zero for the sensing electrodes. More details of the boundary condition or alternative boundary condition can be found in Soleimani and Lionheart (2005).

The electric charge on the lth electrode is given by

$$Q_l = \int_{E_l} \varepsilon \frac{\partial u}{\partial \tilde{n}}\, \mathrm{d}x, \tag{7}$$

where $\tilde{n}$ is the inward normal on the lth electrode.

In an ECT system the capacitance data are usually normalized by calibration data and are given by $\lambda = \frac{C_{\text{meas}} - C_{\text{air}}}{C_{\text{high}} - C_{\text{air}}}$, where C_{air} is the capacitance measurement when the sensor is empty, C_{high} is the capacitance measurement when the sensor is full of a material with high permittivity and C_{meas} is the absolute capacitance measurement.

Usually, FEM is used to solve the forward problem in ECT (Soleimani and Lionheart 2005). To obtain the sensitivity, the Fréchet derivative of the measured capacitance is calculated with respect to a perturbation in permittivity. A simple approach is to ignore the higher order terms. This can simply be extended to a formal proof, using an operator series. A derivation of the sensitivity formula was given in Soleimani and Lionheart (2005) as follows:

$$\frac{\delta Q_{ij}}{\delta \varepsilon_m} = \left\{u_e^i\right\} \left(\int_{\Omega_m} \{\nabla \phi_e\} \cdot \{\nabla \phi_e\}^T\, \mathrm{d}x^2 \right) \left\{u_e^j\right\}, \tag{8}$$

where Ω_m is the perturbed region, ϕ_e is the matrix of the nodal shape function in each element and u_e can be calculated by the solution to the forward problem when electrodes i and j are excited.

2.3. Forward problem in EMT

EMT is based on eddy current measurements. By ignoring the wave propagation effect in Maxwell's equation and by taking $E = -\mathrm{i}\omega A^*$, $A^* - A$ formulation can be used to solve the forward problem in EMT (Biro 1999):

$$\nabla \times \left(\frac{1}{\mu} \nabla \times A^* \right) + \mathrm{i}\omega\sigma A^* = J_0, \tag{9}$$

where J_0 is the current density in the excitation coil, μ is the permeability, σ is the conductivity, A is the magnetic vector potential in free space and A^* is the magnetic vector potential in the conducting region, which includes the gradient of a scalar field (Biro 1999).

The edge FEM has some advantages over other conventional nodal FEM (Bossavit 1999) and has been implemented for solving the forward problem in EMT (Soleimani *et al* 2006). The degrees of freedom are the line integrals of the vector quantities along the edges of a mesh. The interface condition between two elements is satisfied, so that the results from edge-based finite elements are more accurate than those from nodal elements. An incomplete Cholesky conjugate gradient (ICCG) approach has been applied to solve the linear system of equations arising from the edge FEM. Considering that ϕ_i is the nodal scalar basis function, in an edge FEM on a tetrahedral mesh a vector field is represented using a basis of vector-valued functions, where N_{ij} is associated with the edge between nodes i and j:

$$N_{ij} = \phi_i \nabla \phi_j - \phi_j \nabla \phi_i. \tag{10}$$

Galerkin's approximation using edge element basis functions yields

$$\int_{\Omega}\left(\nabla\times N\cdot\frac{1}{\mu}\nabla\times A^{*}\right)\mathrm{d}x^{3}+\int_{\Omega_{\mathrm{e}}}(\mathrm{i}\omega\sigma N\cdot A^{*})\,\mathrm{d}x^{3}=\int_{\Omega_{\mathrm{c}}}(N\cdot J_{0})\,\mathrm{d}x^{3},\tag{11}$$

where N is any linear combination of edge basis functions, Ω is the entire region, Ω_{e} is the eddy current region and Ω_{c} is the current source region.

The current source can be defined by the electric vector potential $J_0 = \nabla\times T_0$, which clearly guarantees that $\nabla\cdot J_0 = 0$. This is important for the convergence of the linear system of equations arising from edge FEM (Biro 1999).

With the A^*-A formulation and using edge FEM, the sensitivity to change in the conductivity of the conducting area can be calculated using the dot product of two electric fields. Considering $E=-\mathrm{i}\omega A^*$, where the integral becomes the inner product of A fields, the Jacobian can be calculated by performing the integration for a chosen basis for the conductivity perturbation $\delta\sigma$. Using the matrix of the shape function in each element $\{N_e\}$ the potential A^* inside each element can be expressed as $A^*=\{N_e\}\cdot\{A_e\}$, where $\{A_e\}$ is defined along edges. The sensitivity term for each element is

$$S=\frac{\partial V_{ij}}{\partial\sigma_m}=-\frac{\omega^2}{I_iI_j}\left\{A_e^i\right\}\left(\int_{\Omega_m}\{N_e\}\cdot\{N_e\}^T\,\mathrm{d}x^3\right)\left\{A_e^j\right\}^T.\tag{12}$$

This expression gives the sensitivity of the pair of coils i, j with an induced voltage to an element. Here, Ω_m is the volume of the element number m and I_i and I_j are excitation currents into the coils. Efficient formulation of the sensitivity formula for EMT has been derived in Soleimani and Lioheart (2006), and sensitivity maps in 3D EMT have been studied in Soleimani (2006).

3. Dynamic image reconstruction

3.1. Time-varying model

In the time-varying estimation approach, the underlying inverse problem can be formulated as a state estimate, so that the dynamic conductivity (or permittivity) distribution can be estimated. Suppose that a measurement has been made at time t_k ($t_k = k\cdot\Delta T$), where k is the discrete time step and ΔT is the sampling interval between two consecutive excitations, and the information, it provides, is applied for updating the state estimate of a system at time t_k. Also suppose that the problem has been discretized with respect to the time variable. In the state estimation problem, the time-varying model is needed, which consists of the state equation for the temporal evolution of the conductivity (or permittivity) distribution and the measurement equation, to present the relationship between the conductivity (or permittivity) distribution and measurements on the boundary. In general, the temporal evolution of the conductivity (or permittivity) distribution p_k in the domain Ω is assumed to be linear:

$$p_{k+1}=F_kp_k+w_k,\tag{13}$$

where F_k is the state transition matrix at time t_k.

Since there is no information on the dynamic behaviour of the process, it is assumed that $F_k = I$ (i.e. identity matrix) for all t_k to obtain the so-called random-walk model. Also, w_k is assumed to be white Gaussian noise with the known covariance matrix $\Gamma_k^w \equiv E\left[w_kw_k^T\right]$, which determines the rate of time evolution in the conductivity distribution.

For the observation model, let V_k be the measurement data induced by the kth excitation pattern. Then the measurement equation can be described as nonlinear mapping with a measurement error as follows:

$$V_k=U_k(p_k)+v_k,\tag{14}$$

where the measurement error v_k is assumed to be white Gaussian noise with known covariance $\Gamma_k^v \equiv E\left[v_kv_k^T\right]$.

By linearizing equation (14) about the nominal value p_0, the following equation is obtained:

$$V_k=U_k(p_0)+J_k(p_0)\cdot(p_k-p_0)+\mathrm{H.O.Ts}+v_k,\tag{15}$$

where H.O.Ts represent the higher order terms, which are assumed to be additional white Gaussian noise, and J_k is the Jacobian matrix defined by

$$J_k(p_0)\equiv\left.\frac{\partial U_k}{\partial p_k}\right|_{p_k=p_0}.\tag{16}$$

Define a pseudo-measurement (artificial measurement) by

$$z_k\equiv V_k-U_k(p_0)+J_k(p_0)\cdot p_0;\tag{17}$$

then the linearized measurement equation is obtained:

$$z_k=J_k(p_0)\cdot p_k+\bar{v}_k,\tag{18}$$

where $\bar{v}_k$ consists of the measurement and linearization errors with the known covariance matrix $\overline{\Gamma}_k^v \equiv E\left[\bar{v}_k\bar{v}_k^T\right]$.

3.2. Inverse problem solver based on the LKF

In the Kalman filtering approach, the state vector p_k is estimated on the basis of a measurement taken up to the time t_k. With the Gaussian assumptions, the estimate is computed by minimizing the following cost functional:

$$\Xi(p_k)=\tfrac{1}{2}\left\{\|p_k-p_{k|k-1}\|^2_{C^{-1}_{k|k-1}}+\|z_k-J_k(p_0)\cdot p_k\|^2_{(\overline{\Gamma}_k^v)^{-1}}+\alpha\|R(p_k-p^*)\|^2\right\},\tag{19}$$

where α and R are the regularization parameter and matrix, respectively, p^* denotes *a priori* information and $C_{k|k-1}$ denotes the time-updated error covariance matrix defined by

$$C_{k|k-1}\equiv E[(p_k-p_{k|k-1})(p_k-p_{k|k-1})^T].\tag{20}$$

The third term on the right side of equation (19) denotes the regularization term that is included to mitigate the ill-conditioned nature of the problem. For the computations, the augmented pseudo-measurement and Jacobian matrices are defined as

$$\bar{z}_k\equiv\begin{bmatrix}z_k\\ \sqrt{\alpha}\cdot R\cdot p^*\end{bmatrix}\tag{21}$$

$$H_k\equiv\begin{bmatrix}J_k(p_0)\\ \sqrt{\alpha}\cdot R\end{bmatrix}.\tag{22}$$

Then the above cost functional can be rewritten as

$$\Xi(\sigma_k)=\tfrac{1}{2}\left\{\|p_k-p_{k|k-1}\|^2_{C^{-1}_{k|k-1}}+\|\bar{z}_k-H_k\cdot p_k\|^2_{\Gamma_k^{-1}}\right\},\tag{23}$$

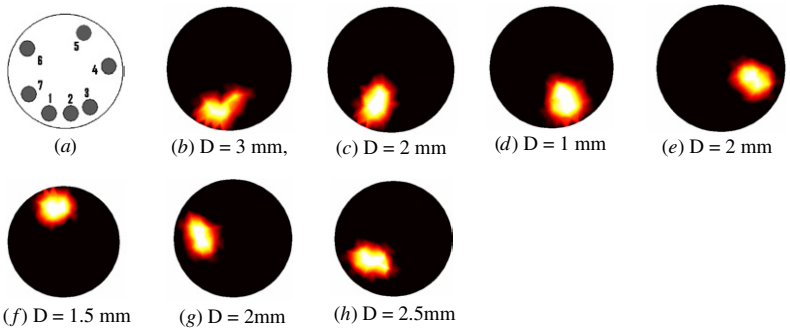

Figure 2. Reconstruction of the moving object using ECT data and the LKF ($a_1 = 10$, $a_2 = 1 \times 10^{-3}$, $\alpha = 1 \times 10^{-1}$), (*a*) moving object, (*b*)–(*h*) images reconstructed using the LKF.

where Γ_k is a block diagonal matrix defined as

$$\Gamma_k \equiv \text{Blockdiag}\left[\overline{\Gamma}_k^v, I\right]. \tag{24}$$

By minimising the cost functional in equation (23), the recursive LKF algorithm is obtained, which consists of the following two steps (Gelb 1974, Grewal and Andrews 2001).

Step 1. Update in measurement (filtering)

$$G_k = C_{k|k-1} \cdot H_k^T \cdot \left[H_k \cdot C_{k|k-1} \cdot H_k^T + \Gamma_k\right]^{-1} \tag{25}$$

$$C_{k|k} = [I_N - G_k \cdot H_k] \cdot C_{k|k-1} \tag{26}$$

$$p_{k|k} = p_{k|k-1} + G_k \cdot [\bar{z}_k - H_k \cdot p_{k|k-1}]. \tag{27}$$

Step 2. Update in time (prediction)

$$C_{k+1|k} = F_k \cdot C_{k|k} \cdot F_k^T + \Gamma_k^w \tag{28}$$

$$p_{k+1|k} = F_k \cdot p_{k|k}. \tag{29}$$

Hence, the estimated state vector $p_{k|k}$ for the true state vector p_k has been found in the sense of a recursive minimum mean square error using the initial guesses, $p_{1|0}$ and $C_{1|0}$. The most interesting feature of the LKF is that the Kalman gain G_k in equation (25) can be computed off-line in advance so that the on-line computational burden is minimal. In the on-line computations of the LKF, only equations (27) and (29) are needed. This effectively eliminates the need to store previous measurements for estimating the present state. In our implementation, the state and the observation noise covariance were diagonal with a_1 and a_2, respectively, on the diagonal. Actually, this is the simplest choice for the covariance and more complicated non-diagonal covariance has been studied earlier (Seppänen *et al* 2001), which could be further implemented for ECT and EMT.

4. Results and discussion

To demonstrate the feasibility and to study the limitation of the LKF, tests have been carried out with ECT using dynamical changes in permittivity and tests with EMT using dynamical changes in conductivity. Both ECT and EMT systems consist of eight sensing electrodes/coils that are equally spaced around the object. In the static imaging mode, the sensors are excited from electrodes 1, 2, ... until electrode 7, and 28 independent measurement data are collected. In ECT an electric potential of 1 V is applied to the excitation electrodes and the charges are measured in the remaining electrodes, which are grounded. In EMT an electric current of 1 A is applied to the excitation coil and induced voltages are measured in the remaining coils, which are open circuit. In this study, the material changes are assumed to be taking place during each excitation. In dynamic image reconstruction in each time step of KF, a set of seven measured data corresponding to one excitation is used. Each image frame is reconstructed using seven measurement data from one excitation. For the experiment, the object was moved, and the recorded data were related to a single excitation. The distance between the centres of reconstructed and real object (D) is an objective measure for the reconstruction algorithm.

4.1. ECT results

For image reconstruction with ECT, a 2D triangular mesh including $N = 422$ elements in the region of interest was used. Note that this is the number of elements inside a circular region of diameter 100 mm as the imaging region. The number of measurements in each excitation is $L = 7$. A plastic rod with a permittivity of 1.8 and diameter of 12 mm was used as an inclusion. Figure 2 shows the dynamic reconstruction of the object movement using the LKF. Figure 3 shows the reconstruction of the same plastic object movement towards the centre using the LKF. Figures 3(*a*) and 4(*a*) show the pattern of the movement of the rod. Of many experimental tests, two cases have been chosen to show the reconstruction with a random movement (especially in the example in figure 2) to make sure that the algorithm is not biased with a systematic object movement.

Figure 4 shows the singular value plot of the Jacobian with the whole data set with 28 measurements and one excitation data set (i.e. seven data). As the singular value plot shows, without temporal and spatial regularization the inverse problem with the whole data set can generate more features than a single pattern, and the number of a singular value participating in image reconstruction is higher than that with the whole data set, for a normal noise level. If the changes happen within the measuring period, the dynamic approach has to be used; the temporal correlation between the frame considered for dynamic reconstruction and spatial regularization enables the temporal changes in permittivity to be imaged.

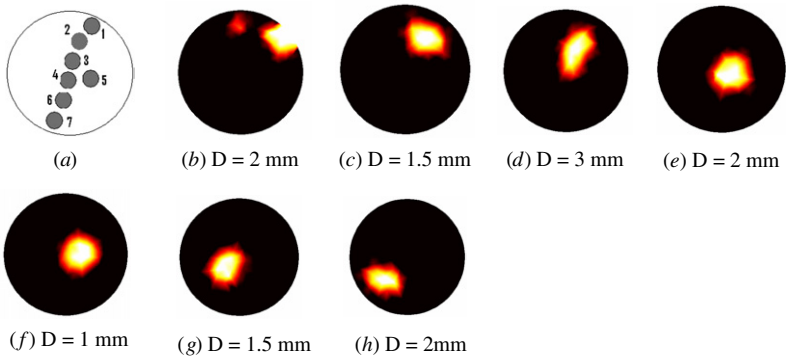

Figure 3. Reconstruction of the moving object using ECT data and the LKF ($a_1 = 10$, $a_2 = 1 \times 10^{-3}$, $\alpha = 1 \times 10^{-1}$), (*a*) moving object, (*b*)–(*h*) images reconstructed using the LKF.

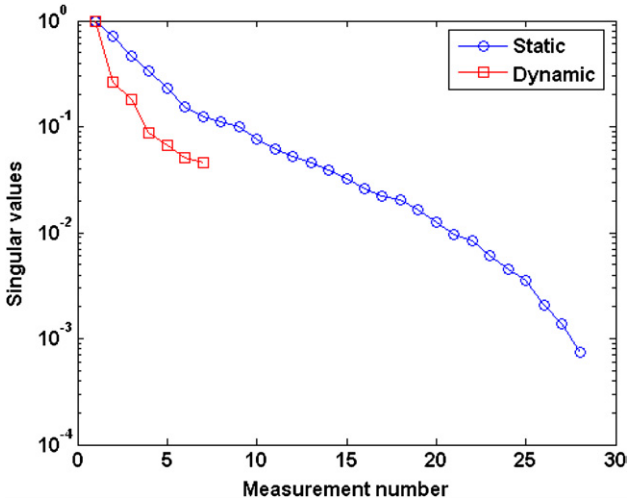

Figure 4. Singular value plot of Jacobian for 28 data set and 7 data of excitation of electrode 1, both for free space.

It is suggested that more dominant singular values in a whole data set are more distributed in the imaging area, and the single excitation scheme is more biased towards the area closer to the excitation electrodes. This effect may be less problematic in a multiple excitation tomography system, such as an ACT system (Kim *et al* 2006). In this study one excitation per frame is not used in an assumption that the movement of the object is faster than one frame of a whole data set. If a whole data set is collected, it would be corrupted and completely incorrect images produced.

4.2. EMT results

For image reconstruction in EMT, a 3D tetrahedral mesh was used with $N = 2832$ elements in the region of interest. The number of measurements in each excitation is $L = 7$. The diameter of the imaging area is 160 mm. In figure 5, the images only show a cross section of the 3D images in the plane $z = 0$ and the reconstruction of the radial movement of the copper rod with a diameter of 19 mm. In this case the copper rod is reconstructed using the LKF, where the object moved to seven different locations, starting in the front of coil 5 and moving 45° anticlockwise in each step. Figure 6 shows the reconstruction of the movement of the same copper bar from the left to the centre. In this test the object starts from (−70 mm, 0) and moves 9.5 mm towards the centre in each step.

The choice of the parameters (a_1, a_2 and α) and the initial state of the image has an influence upon the quality of the dynamic image reconstruction. The noise covariance can be measured and the noise level on each measurement channel

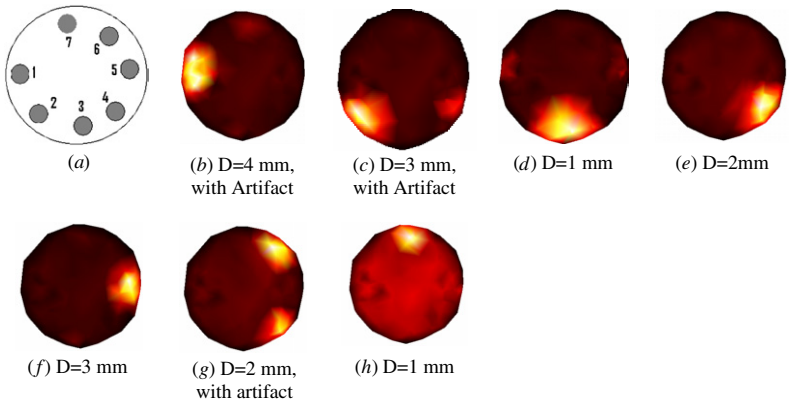

Figure 5. Reconstruction of the moving object using EMT data and the LKF ($a_1 = 10$, $a_2 = 1 \times 10^{-3}$; $\alpha = 1 \times 10^{-1}$), (*a*) moving object, (*b*)–(*h*) images reconstructed using the LKF.

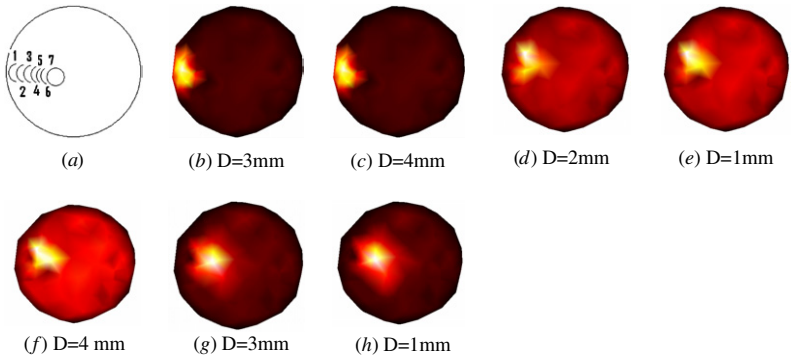

(*a*) (*b*) D=3mm (*c*) D=4mm (*d*) D=2mm (*e*) D=1mm

(*f*) D=4 mm (*g*) D=3mm (*h*) D=1mm

Figure 6. Reconstruction of the moving object using EMT data and the LKF ($a_1 = 10$, $a_1 = 1 \times 10^{-3}$, $\alpha = 1 \times 10^{-1}$), (*a*) moving object, (*b*)–(*h*) images reconstructed using the LKF.

controlled by a_2. The state noise value, which is controlled by a_1, controls how fast the method follows the temporal changes. The smaller the elements of the state noise covariance are, the slower the estimates change. The so-called lag error of the algorithm is large in this case. If the elements of the state noise covariance are large, the lag error diminishes but the estimates are noisier. On the other hand, α controls the spatial smoothness of the reconstructed image for each time step.

While an optimal choice of these parameters needs to be studied, all reconstruction results presented in this paper are obtained using similar parameters. The main source of artefacts specially in images in figure 5 is due to the choice of these parameters and different shapes of the sensitivity map in EMT (Scharfetter *et al* 2002). The initial guess for the material distribution in all cases is the free space, with a relative permittivity of 1 for ECT and conductivity 0 for EMT. Despite good images, in the first few steps in these examples, the shape of the object cannot be reconstructed using the LKF with a given initial image state, but the temporal resolution is improved as demonstrated. This would not be achieved if the static image reconstruction had been used. The data acquisition rate of the EMT system used in this study is 10 frame s^{-1} (Ma *et al* 2006) and that of the ECT system is 120 frame s^{-1} (Yang 1996). In either case, if the material movement is faster than the data acquisition rate, the static imaging method will not be able to capture that movement, whereas the dynamic imaging method could improve the speed of the imaging by a factor of 8. In both ECT and EMT the measured data were normalized, and thresholds were applied to the reconstructed images, 1 and 1.5 to the ECT images and 0 and 5000 to the EMT images.

5. Conclusions

In many applications of ECT and EMT, the permittivity, conductivity and/or permeability distributions may change so fast that the time-varying information is either lost or severely blurred, if a full set of independent excitation patterns is applied for image reconstruction. An example is flow visualization, in which both ECT and EMT systems have been used. In many cases the material passes faster than an imaging system can collect all the measurement data. In this paper, a time-varying image reconstruction algorithm for ECT and EMT is presented, aiming to estimate rapidly changing permittivity, conductivity and/or permeability distributions. The experimental results show that the dynamic imaging method with the LKF produces satisfactory results in tracking time-varying ECT and EMT data. In this study, the LKF has been demonstrated as the first step for time-varying imaging.

Although the LKF can be very fast and efficient for real-time imaging, it has some drawbacks of treating the nonlinear problem as linear reconstruction. A future work is to take into account the nonlinearity of the inverse problem, e.g. using a particle filter as studied in Watzenig *et al* (2007) or extended Kalman filtering.

References

Biro O 1999 Edge element formulations of eddy current problems *Comput. Methods Appl. Mech. Eng.* **169** 391–405

Bossavit A 1999 *Computational Electromagnetism* (Boston: Academic)

Gelb A 1974 *Applied Optimal Estimation* (Cambridge MA: MIT Press)

Grewal M S and Andrews A P 2001 *Kalman Filtering: Theory and Practice, Using MATLAB* (New York: Wiley)

Griffiths H 2001 Magnetic induction tomography *Meas. Sci. Technol.* **12** 1126–31

Ijaz U Z, Kim J H, Kim M C, Kim S, Park J W and Kim K Y 2006 Nondestructive dynamic process monitoring using electrical capacitance tomography *Key Eng. Mater.* **321–323** 1671–4

Kim B S, Kim K Y, Kao T-J, Newell J C, Isaacson D and Saulnier G J 2006 Dynamic electrical impedance imaging of a chest phantom using the Kalman filter *Physiol. Meas.* **27** S81–91

Kim K Y, Kim B S, Kim M C and Kim S 2004 Dynamic inverse obstacle problems with electrical impedance tomography *Math. Comput. Simul.* **66** 399–408

Ma X, Peyton A J, Higson S R, Lyons A and Dickinson S J 2006 Hardware and software design for an electromagnetic induction tomography (EMT) system for high contrast metal process applications *Meas. Sci. Technol.* **17** 111–8

Merwa R, Hollaus K, Brunner P and Scharfetter H 2005 Solution of the inverse problem of magnetic induction tomography (MIT) *Physiol. Meas.* **26** S241–50

Scharfetter H, Riu P, Populo M and Rosell J 2002 Sensitivity maps for low-contrast-perturbations within conducting background in magnetic induction tomography (MIT) *Physiol. Meas.* **23** 195–202

Seppänen A, Heikkinen L, Savolainen T, Voutilainen A, Somersalo E and Kaipio J P 2007 An experimental evaluation of state estimation with fluid dynamical models in process tomography *Chem. Eng. J.* **127** 23–30

Seppänen A, Vauhkonen M, Somersalo E and Kaipio J P 2001 State space models in process tomography: approximation of state noise covariance *Inverse Problems Eng.* **9** 561–85

Soleimani M 2006 Sensitivity maps in three-dimensional magnetic induction tomography Insight *Non-Destr. Test. Cond. Monit.* **48** 39–44

Soleimani M and Lionheart W R B 2005 Nonlinear image reconstruction in electrical capacitance tomography using experimental data *Meas. Sci. Technol.* **16** 1987–96

Soleimani M and Lionheart W R B 2006 Absolute conductivity reconstruction in magnetic induction tomography using a nonlinear method *IEEE Trans. Med. Imaging* **25** 1521–30

Soleimani M, Lionheart W R B, Peyton A J, Ma X and Higson S 2006 A 3D inverse finite element method applied to the experimental eddy current imaging data *IEEE Trans. Magn.* **42** 1560–7

Vauhkonen M, Karjalainen P A and Kaipio J P 1998a A Kalman filter approach to track fast impedance changes in electrical impedance tomography *IEEE Trans. Biomed. Eng.* **45** 486–93

Vauhkonen M, Vaduasz D, Karjalainen P A, Somersalo E and Kaipio J P 1998b Tikhonov regularization and prior information in electrical impedance tomography *IEEE Trans. Med. Imaging* **17** 285–93

Vauhkonen P J, Vauhkonen M, Muakinen T, Karjalainen P A and Kaipio J P 2000 Dynamic electrical impedance tomography phantom studies *Inverse Problems Eng.* **8** 495–510

Watzenig D, Brandner M and Steiner G 2007 A particle filter approach for tomographic imaging based on different state-space representations *Meas. Sci. Technol.* **18** 30–40

Watzenig D, Steiner G and Brandstatter B 2004 Managing noisy measurement data by means of statistical parameter estimation in electrical capacitance tomography *Proc. 11th Int. IGTE Symp. on Numerical Field Calculation in Electrical Engineering (Graz-Seggauberg, Austria)* pp 196–201

Yang W and Peng L 2003 Image reconstruction algorithms for electrical capacitance tomography *Meas. Sci. Technol.* **14** R1–13

Yang W Q 1996 Hardware design of electrical capacitance tomography systems *Meas. Sci. Technol.* **7** 225–32